A Frictional Skeleton Model for the Madden–Julian Oscillation*

FEI LIU AND BIN WANG

International Pacific Research Center, and Department of Meteorology, University of Hawaii at Manoa, Honolulu, Hawaii

(Manuscript received 14 January 2012, in final form 15 April 2012)

ABSTRACT

The Madden–Julian oscillation (MJO) is a multiscale system. A skeleton model, developed by Majda and Stechmann, can capture some of planetary-scale aspects of observed features such as slow eastward propagation, nondispersive behavior, and quadrupole-vortex structure. However, the Majda–Stechmann model cannot explain the source of instability and the preferred planetary scale of the MJO. Since the MJO major convection region is leaded by its planetary boundary layer (PBL) moisture convergence, here a frictional skeleton model is built by implementing a slab PBL into the neutral skeleton model. As a skeleton model allowing the scale interaction, this model is only valid for large-scale waves. This study shows that the PBL frictional convergence provides a strong instability source for the long eastward modes, although it also destabilizes very short westward modes. For the long waves (wavenumber less than 5), the PBL Ekman pumping moistens the low troposphere to the east of the MJO convective envelope, and sets up favorable moist conditions to destabilize the MJO and favor only eastward modes. Sensitivity experiments show that a weak PBL friction will enhance the instability slightly. The sea surface temperature (SST) with a maximum at the equator also prefers the long eastward modes. These theoretical analysis results encourage further observations on the PBL regulation of mesosynoptic-scale motions, and exploration of the interaction between PBL and multiscale motions, associated with the MJO to improve the MJO simulation in general circulation models (GCMs).

1. Introduction

The Madden–Julian oscillation (MJO), named after its discoverers (Madden and Julian 1971, 1972, 1994), features an equatorially trapped, slowly eastward-propagating (about 5 m s^{-1}), planetary-scale baroclinic circulation cell in the Eastern Hemisphere (Knutson and Weickmann 1987; Wang and Rui 1990; Hendon and Salby 1994; Maloney and Hartmann 1998; Kiladis et al. 2005; Zhang 2005). The MJO circulation comprises equatorial Kelvin waves and Rossby waves, and exhibits a quadrupole-vortex horizontal structure when the MJO convection is located over the equatorial Indian Ocean and the western Pacific (Rui and Wang 1990; Hendon and Salby 1994). A phase lag usually occurs between the leading planetary boundary layer (PBL) moisture convergence and the midtropospheric counterparts (Hendon and Salby 1994; Sperber 2003). Meanwhile, the MJO also presents nondispersity (Salby and Hendon 1994; Wheeler and Kiladis 1999; Roundy and Frank 2004).

Recent observations show that the MJO is usually coupled with a multiscale convective complex (Nakazawa 1988; Hendon and Liebmann 1994; Houze et al. 2000; Slingo et al. 2003; Straub and Kiladis 2003; Haertel and Kiladis 2004; Moncrieff 2004; Kikuchi and Wang 2010). Multicloud models (Khouider and Majda 2007; Majda et al. 2007; Khouider and Majda 2008; Khouider et al. 2011) and multiscale models (Majda and Biello 2004; Biello and Majda 2005; Biello et al. 2007; Majda and Stechmann 2009a; Wang and Liu 2011; Liu and Wang 2011, 2012; Liu et al. 2011) have been built to study the multiscale nature of the MJO.

Based on the multiscale structures of the MJO, the primary instabilities and damping are assumed to occur on synoptic scales (Khouider and Majda 2006, 2008; Kiladis et al. 2009). By the key premise that modulations

* School of Ocean and Earth Science and Technology Contribution Number 8669, and International Pacific Research Center Publication Number 885.

Corresponding author address: Dr. Bin Wang, IPRC and Department of Meteorology, University of Hawaii at Manoa, 401 Post Bldg., 1680 East-West Road, Honolulu, HI 96822.
E-mail: wangbin@hawaii.edu

DOI: 10.1175/JAS-D-12-020.1

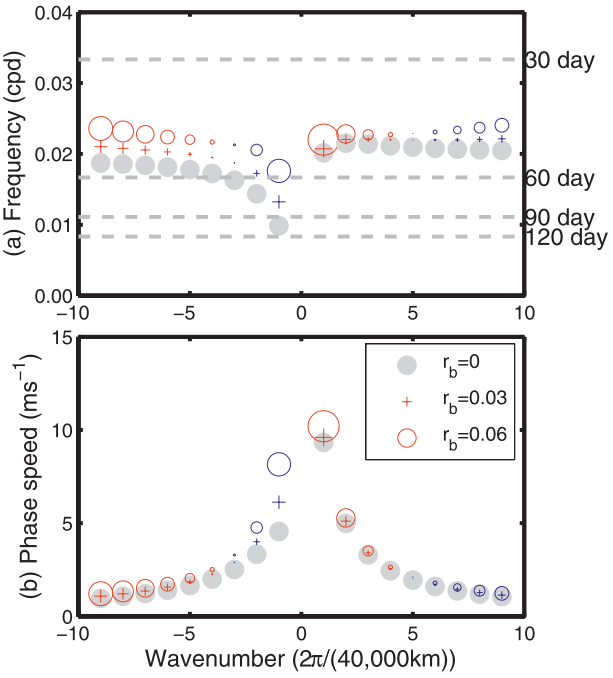

FIG. 1. (a) Frequency and (b) phase speed as a function of wavenumber for low-frequency modes of the skeleton model. Gray dots denote results of MS09 without the PBL effect, $r_b = 0$. Crosses and circles denote results derived from the frictional skeleton model with $r_b = 0.03$ and $r_b = 0.06$, respectively. Red and blue denote unstable and damped modes, respectively. The growth rates are proportional to the diameters, with respect to the maximum growth rate of 0.11 day^{-1}.

of synoptic-scale wave activity are included by low-level moisture preconditioning on planetary scales, Majda and Stechmann (2009b; hereafter MS09) parameterized these scale interactions and presented a general skeleton model for the MJO, which captured three important features of the MJO skeleton: 1) slow eastward propagation at a speed of roughly 5 m s^{-1} (Fig. 1b); 2) peculiar dispersion relation of $d\omega/dk \approx 0$ (Fig. 1a), where ω and k are the frequency and wavenumber, respectively; and 3) quadrupole-vortex horizontal structure (Fig. 2). However, the MS09 model only produces neutral modes and does not explain why the MJO skeleton can grow or be maintained against thermal and momentum damping, or why faster growth occurs on the preferred planetary scale.

Observations and general circulation model (GCMs) simulations show that the MJO major convection region is leaded by its PBL moisture convergence (Wang 1988; Hendon and Liebmann 1994; Hendon and Salby 1994; Jones and Weare 1996; Maloney and Hartmann 1998; Matthews 2000; Sperber 2003; Lin et al. 2004; Tian et al. 2006; Yang et al. 2008). This vertical tilted structure is one of the fundamental features of the MJO and has important implications for MJO dynamics. Wang (1988) demonstrated that low-frequency, moist equatorial Kelvin waves are driven by an instability arising from the PBL-induced moisture convergence. Frictional moisture convergence–induced heating was shown to be able to couple with the equatorial Kelvin and Rossby waves and select a slow eastward movement for the coupled Kelvin–Rossby wave packet (Wang and Rui 1990). However, in their works (Wang 1988; Wang and Rui 1990), the moisture pumped by the PBL was parameterized directly into the diabatic heating, without considering scale interaction. When coupled with the multicloud model of Khouider and Majda (2006), the PBL can amplify greatly the convectively coupled Kelvin waves (Waite and Khouider 2009). The frictional moisture convergence mechanism has also been confirmed further in more complex models, with different convective parameterization schemes (Salby et al. 1994; Ohuchi and Yamasaki 1997; Moskowitz and Bretherton 2000). These results encourage us to study the role of the PBL in sustaining the MJO skeleton.

To understand the role of the PBL in sustaining the MJO skeleton, we try to build a frictional skeleton model, where a slab PBL is implemented into the MS09 skeleton model (section 2). In section 3, we present a new instability source for the MJO skeleton, arising from the interaction between the boundary layer dynamics and the MJO skeleton, and discuss the preferred eastward propagation and long-wave selection for the MJO. The role of the equatorially trapped sea surface temperature (SST) on selecting the eastward propagation of the MJO is also discussed in section 4. The last section summarizes the results, and discusses limitations and future work.

2. The frictional MJO skeleton model

a. The neutral skeleton model for the MJO

The neutral skeleton model was proposed by MS09 and developed further by Majda and Stechmann (2011). In this skeleton model, the effects of synoptic wave activity (and upscale eddy moisture and heat transfer) are parameterized in the planetary-scale temperature and moisture equations, which drive the MJO skeleton. The recent works of Liu and Wang (2011, 2012) demonstrate that the out-of-phase eddy heat and moisture transfer supports this parameterized relationship between the temperature and moisture dynamics. They showed that, on planetary scales, the westward-propagating 2-day waves provide negative eddy heat transfer but positive eddy moisture transfer, and the eastward-moving moist Kelvin waves provide positive eddy heat transfer but

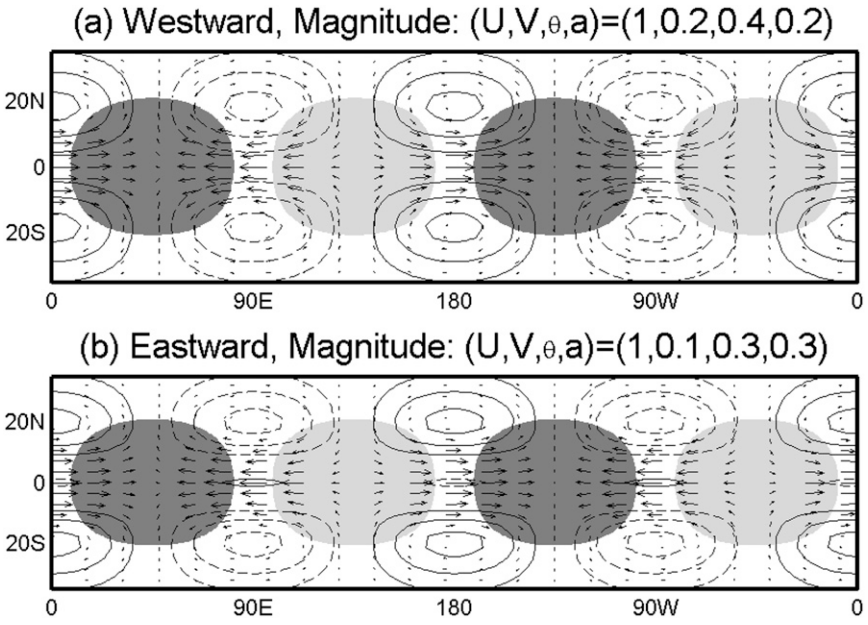

FIG. 2. Velocity vectors, wave activity (shading), with lower-tropospheric temperature (contours) of the neutral (a) westward and (b) eastward modes are plotted for wavenumber 2, where $r_b = 0$. Positive (negative) contours are solid (dashed), and positive (negative) shading is dark (light) gray. Contour interval is one-third of the magnitude, and zero contours are not drawn. Only wave activity above one-third of the magnitude is shaded.

negative moisture transfer. In this skeleton model, only the amplitude of wave activity, rather than details of synoptic-scale motion, is considered.

To form a closed system of the skeleton model, parameterization of the interaction between large-scale moisture anomaly q and the wave activity a is necessary. By assuming that the temporal tendency of the wave activity is determined by the moisture anomaly, the simplest equation for this interaction is given by

$$a_t = \Gamma q a, \tag{1}$$

where Γ is a constant of proportionality: positive lower-tropospheric moisture anomaly favors the growth of the synoptic-scale wave activity. A series of observations, modeling, and theories support the idea of (1) (Majda and Stechmann 2011).

This skeleton model is formulated in terms of anomalies from a uniform base state of radiative–convective equilibrium $\overline{R} = \overline{H}\overline{a}$, where $\overline{R} = 1\,\mathrm{K\,day^{-1}}$ is the fixed constant radiative cooling rate, $\overline{H}$ is a constant heating rate prefactor, and $\overline{a}$ is a constant (nondimensional) amplitude of wave activity in the equilibrium state. Taking $C = 50\ \mathrm{m\ s^{-1}}$ (the lowest internal gravity wave speed) as the reference speed, and the characteristic temporal and spatial scales as $\sqrt{1/C\beta} = 8.5$ h and $\sqrt{C/\beta} = 1500$ km, respectively, where β represents the leading-order curvature effect of the earth at the equator, the nondimensional MJO skeleton model can be obtained by combining the parameterization (1) with the linearized primitive equations:

$$\begin{aligned} u_t - yv &= -p_x, \\ yu &= -p_y, \\ 0 &= -p_z + \theta, \\ u_x + v_y + w_z &= 0, \\ \theta_t - w &= \overline{H}a, \\ q_t - \tilde{Q}w &= -\overline{H}a, \\ a_t &= \Gamma q(\overline{a} + a), \end{aligned} \tag{2}$$

where u, v, and w are the zonal, meridional, and vertical velocities, and p and θ are the pressure and potential temperature, respectively. The nondimensional vertical gradient of the background moisture $\tilde{Q}$ is taken as 0.9, the standard value for the low-frequency motions (Yano and Emanuel 1991; Frierson et al. 2004; MS09; Majda and Stechmann 2011) ($\approx 0.2\ \mathrm{K^{-1}\ day^{-1}}$ in dimensional units), where Γq acts as a dynamic growth/decay rate of the wave activity envelope, in response to the moisture anomaly.

The simplest linear model for the MJO can be truncated vertically on the first baroclinic mode, that is, $u(x, y, z, t) = u'(x, y, t)\sqrt{2}\cos(z)$, etc. The nonlinear

process in (1) is not studied here, and the resulting equations resemble a time-dependent version of a Matsuno–Gill model (Matsuno 1966; Gill 1980):

$$\begin{aligned} u_t - yv + p_x &= 0,\\ yu + p_y &= 0,\\ p_t + u_x + v_y &= -\overline{H}a,\\ q_t + \tilde{Q}(u_x + v_y) &= -\overline{H}a,\\ a_t &= \Gamma\bar{a}q. \end{aligned} \tag{3}$$

For simplicity, the primes for the first baroclinic mode are omitted.

b. The PBL

In observation, under the strong lower-tropospheric easterly winds associated with the low pressure anomaly of the MJO, the PBL exhibits prevailing equatorward winds and produces strong convergence that precedes the major convection region of the MJO (Hendon and Salby 1994). This can be represented by a dynamical PBL model. The PBL has a strong friction E with a time scale of about 0.5 day^{-1}, the full linear and barotropic equations of the PBL can be written as

$$\begin{aligned} u_{bt} - yv_b &= -p_{bx} - Eu_b,\\ v_{bt} + yu_b &= -p_{by} - Ev_b. \end{aligned} \tag{4}$$

The variables p_b, u_b, and v_b respectively denote the pressure and zonal and meridional velocities of the PBL. For a specified MJO-like pressure anomaly with the form of

$$p_b = \exp\{-[(x - 120°)/60°]^2\}\exp[-(y/10°)^2]. \tag{5}$$

The PBL field can be easily calculated under this specified pressure forcing. The magnitude ratio (from output at 30 days when the model reaches a steady state) of v_b to u_b is 1.4 and 0.25 according to different E of 0.5 and 10 day^{-1}, respectively. This result means that the strong frictional PBL will produce comparable u and v for an MJO-like low pressure anomaly, while the free troposphere has much stronger zonal winds, so the PBL will produce strong convergence and excite the Ekman pumping. Since the MJO has a period of about 30 days, E has a scale of about 0.5 day^{-1}, and the temporal variant term u_{bt} and v_{bt} in (4) can be omitted by scale analysis. The nondimensional steady PBL model can be written as (Wang and Li 1994)

$$\begin{aligned} -yv_b &= -p_{bx} - Eu_b,\\ yu_b &= -p_{by} - Ev_b,\\ \frac{H_b}{H_T}(u_{bx} + v_{by}) + w_b &= 0. \end{aligned} \tag{6}$$

The term E is selected to represent a damping of one-third of a day, and its nondimensional value is 1.1. The boundary layer depth $H_b = 1$ km and troposphere depth scale is $H_T = 16/\pi = 5.1$ km (Majda and Biello 2004). Also, p_b is assumed to match the pressure of the free troposphere baroclinic mode, which has the form of $\cos(z)$ and a pressure anomaly p at the top of the PBL (i.e., $p_b = p$). The nondimensional Ekman pumping can be calculated from (6):

$$w_b = \frac{H_b}{H_T}(d_1\nabla^2 p_b + d_2 p_{bx} + d_3 p_{by}), \tag{7}$$

where $d_1 = E/(E^2 + y^2)$, $d_2 = -(E^2 - y^2)/(E^2 + y^2)^2$, and $d_3 = -2Ey/(E^2 + y^2)^2$. The moisture coming from the Ekman pumping can be written as (Wang 1988)

$$m_b = w_b(q_b - q_c), \tag{8}$$

where q_b and q_c are the nondimensional mean moisture of the PBL and lower troposphere, and they are defined by $q_b = L_q\int_0^{H_b} q(z)\,dz/(C^2/RC_pH_b)$ and $q_c = L_q\int_{H_b}^{H_b+H_T} q(z)\,dz/(C^2/RC_pH_T)$, respectively. Also, $C_p = 1004$ J kg^{-1} K^{-1} is the specific heat at constant pressure, $R = 287$ J kg^{-1} K^{-1} is the specific gas constant, and $L_q = 2.5 \times 10^6$ J kg^{-1} is the latent heat of condensation. The basic-state specific humidity $q(z)$ is assumed to decrease upward exponentially from q_s at the surface, with an e-folding scale (water vapor density scale height) of 2.2 km (Wang 1988). The value of q_s is estimated based on an empirical dependence on the sea surface temperature θ_s: $q_s = (0.972\theta_s - 8.92) \times 10^{-3}$ kg kg^{-1} (Li and Wang 1994).

This moisture source m_b can be added easily into the moisture equation, then the frictional skeleton model becomes

$$\begin{aligned} u_t - yv + p_x &= 0,\\ yu + p_y &= 0,\\ p_t + u_x + v_y &= -\overline{H}a,\\ q_t + \tilde{Q}(u_x + v_y) &= -\overline{H}a + r_b(\theta_s - 9.18)w_b,\\ \alpha_t &= \Gamma\bar{a}q, \end{aligned} \tag{9}$$

where the standard PBL coefficient $r_b = (0.972 \times 10^{-3} \times L_q/C^2/RC_p)\{\int_0^{H_b}[e^{-z/(2.2\,\mathrm{km})}/H_b]\,dz - \int_{H_b}^{H_b+H_T}[e^{-z/(2.2\,\mathrm{km})}/H_T]\,dz\} = 0.06$. In this paper we use $\theta_s = 28.5$°C.

c. Eigenvalue problem

Equations (7) and (9) compose a set of linear partial differential equations, for which the eigenvalue problem can be readily solved. For the zonal propagating plane waves, we assume that they have the structure of $e^{i(kx-\sigma t)}$,

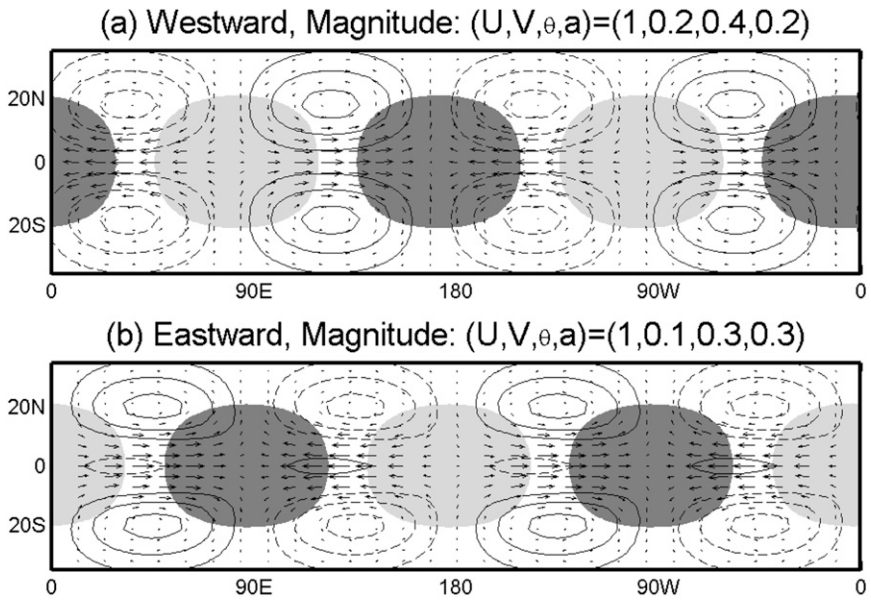

FIG. 3. As in Fig. 2, but for the frictional modes, where $r_b = 0.06$.

where k is the wavenumber and σ is the frequency. The phase speed and growth rate are defined by $\mathrm{Re}(\sigma)/k$ and $\mathrm{Im}(\sigma)$, respectively.

When only the lowest N meridional modes of each variable are kept for the meridional expansion of parabolic cylinder functions, we project (7) and (9) on to the σ–k space and obtain a linear matrix of $(5N \times 5N)$ for the five variables in (9). Here $N = 1$ represents the lowest equatorially trapped mode. The frequency and eigenvectors are calculated through the matrix inversion corresponding to each wavenumber. Only the Kelvin and Rossby waves are kept in (9) because of the long-wave approximation in the free troposphere. Following the idea that the wave activity has only the lowest meridional truncation of parabolic cylinder functions (MS09), the Rossby and Kelvin waves, on their lowest meridional modes, can be studied by using $N = 3$, and sensitive experiments show that a higher N does not affect the results.

To derive this skeleton model, the multiscale processes are included in the wave activity implicitly (MS09), so this frictional skeleton model is only valid for the long waves. In this paper, we only present the results with wavenumber smaller than 10.

3. The instability mechanism

When the PBL is included, the frictional model still captures the MJO-like features that the original neutral model (MS09) produced (Figs. 1 and 3). The inclusion of the PBL, however, makes the eastward-propagating long waves and westward-propagating short waves unstable, while the westward-moving long waves and eastward-moving short waves become damped (Fig. 1). For eastward modes, the strongest instability is associated with wavenumber 1; for westward modes, the growth rate increases as wavelength decreases, and the ''ultraviolet catastrophe'' problem exists for short westward modes. This result indicates, at least on planetary scales, that the PBL prefers the eastward-propagating mode. This result is consistent with the findings of Wang and Rui (1990), namely that the PBL provides an instability source to couple the eastward Kelvin waves and westward Rossby waves, and results in coupled eastward-moving modes when only considering the planetary modes. Coupled with the same PBL, the nonlinear heating in a two-layer model can select the most unstable planetary-scale eastward modes (Li and Zhou 2009).

The sensitivity experiment with a weaker PBL coefficient, for example $r_b = 0.03$ associated with a smaller PBL depth, yields the same qualitative results, except that the growth rates are reduced (Fig. 1). Decreasing sea surface temperature also plays the same role as the weak PBL coefficient did.

The role of the PBL mainly comes from E, and sensitivity experiments show that a small E still maintains the similar behavior of the MJO skeleton (Figs. 1 and 3), except that the growth rates are enhanced. The growth rate of eastward wavenumber 1 is 0.08, 0.11, 0.13, and 0.14 day^{-1} for E with damping scales of 4, 8, and 16 h and of 1 day, respectively.

For the growing modes, positive available potential energy (APE) should be generated, which requires

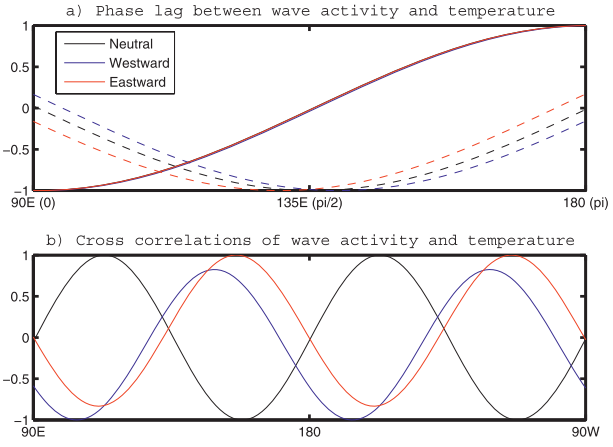

FIG. 4. Relationship between the wave activity and temperature perturbations for wavenumber 2. (a) Phase lag between the meridionally averaged wave activity (dashed) and temperature perturbation (solid). For comparison, the results are shifted zonally so that the zero temperature anomalies are all located at 90°E. (b) Cross correlation ($\overline{Ha\theta}$) of the wave activity and temperature perturbation along the equator. Perturbations are all normalized by their magnitudes. Black, blue, and red denote neutral (Fig. 2), damped westward (Fig. 3a), and unstable eastward (Fig. 3b) modes, respectively.

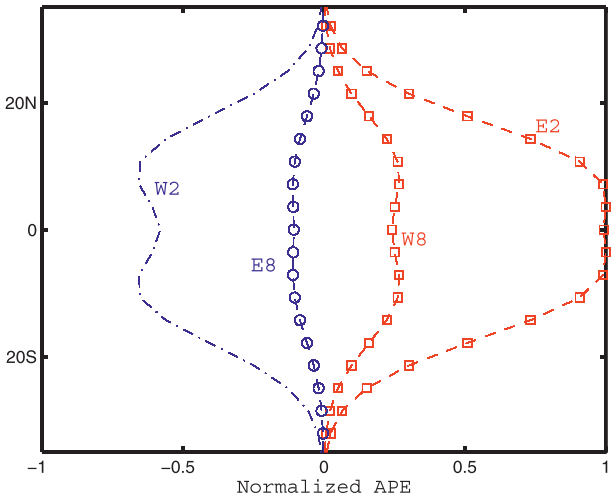

FIG. 5. Normalized available potential energy (APE) for eastward (E) and westward (W) modes with wavenumbers 2 and 8, respectively. APE is normalized by the maximum APE of the eastward wavenumber-2 mode.

positive covariance between the perturbation temperature and wave activity (diabatic heating), or $\overline{\theta}\overline{Ha}$ averaged in one wavelength (Wang and Rui 1990). In the neutral model of MS09, the perturbation wave activity and temperature have a $\pi/2$ phase difference (Figs. 2 and 4a), thus no APE can be generated (Fig. 4b). While the presence of the PBL alters the phase relationship between the wave activity and temperature anomalies; for example, the perturbation wave activity is ahead of the temperature anomaly by a phase larger than $\pi/2$ for the westward mode (Figs. 3a and 4a), and by a phase smaller than $\pi/2$ for the eastward mode (Figs. 3b and 4a). Thus, positive APE is generated for eastward long waves, while APE is negative for westward long waves (Figs. 4b and 5).

How is APE generated? Figures 6 and 7 show that generation comes from the additional moisture source pumped by the PBL. Since the PBL excites wavelength-dependent Ekman pumping (Li and Wang 1994), for long waves, the right-hand side (rhs) terms in (7) containing zonal derivatives are small compared to the remaining terms, $w_b \propto (d_1 p_{byy} + d_3 p_{by})$, and the Ekman pumping is determined primarily by the meridional variation of the pressure anomaly. As shown in Fig. 3, the pressure anomalies, as well as the temperature anomalies, are in phase with off-equatorial cyclones and have strongest variation near the equator, so the Ekman pumping is equatorially trapped and is in phase with the zonal winds. In contrast, for short waves, $w_b \propto (-k^2 d_1 + ikd_2)p_b$, the Ekman pumping is controlled mainly by the strong off-equatorial pressure and is in phase with the cyclones (Fig. 7).

For the long eastward mode, the positive equatorially trapped Ekman pumping leads the wave activity and prepares additional moisture for the growth of the wave activity (Fig. 6b), whereas for long westward mode the negative equatorial Ekman pumping damps it by drying the lower troposphere in front of the wave activity (Fig. 6a). For short waves, the strong off-equatorial Ekman pumping, located to the west of the wave activity (Fig. 7), fulfills an opposite role, namely damping the eastward mode and destabilizing the westward mode.

4. The role of the equatorially trapped SST

In the above section, this model presents that the instability for short westward modes increases with decreasing wavelength. Even for westward wavenumber 10, the PBL produces a considerable instability compared to the eastward wavenumber 1 (Fig. 1a). But this result is obtained by calculating the model with constant SST of 28.5°C. In observation, SST has usually an equatorial maximum and decays poleward, especially in the boreal wintertime when the MJO prevails (Zhang 2005). So we further take a look at the role of the SST in this frictional skeleton model. Two additional sensitivity experiments have been run, where $\tilde{Q} = \tilde{Q}_0 \exp[-(y/y_L)^2]$ and $\theta_s = \theta_0 \exp[-(y/y_L)^2]$. To compare the role of the meridional variation of the SST, we select $\theta_0 = 28.5$°C and $\tilde{Q}_0 = 0.9$ when $y = \infty$ and $\theta_0 = 31.0$°C and $\tilde{Q}_0 = 0.98$

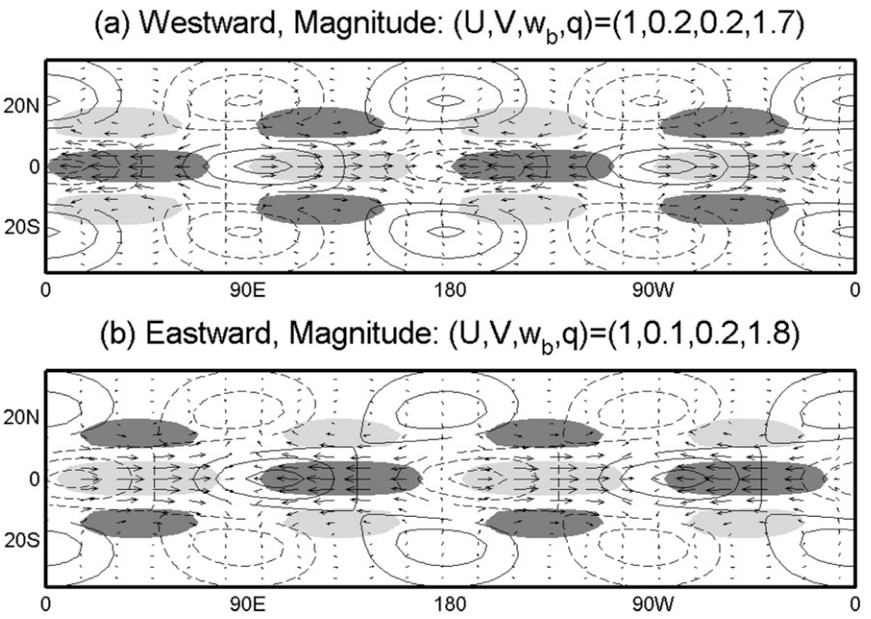

FIG. 6. Velocity vectors, lower-tropospheric moisture (contours), and Ekman pumping (shading) of the (a) westward and (b) eastward modes are plotted for wavenumber 2, where $r_b = 0.06$. Positive (negative) contours are solid (dashed), and positive (negative) shading is dark (light) gray. Contour interval is one-third of the magnitude, and zero contours are not drawn. Only Ekman pumping above one-third of the magnitude is shaded.

when $y = 20°$. The stronger SST magnitude is chosen for the equatorially trapped SST, to make sure that the equatorial region (15°S–15°N) has the same meridional averaged SST, and the meridional averaged gross moist statics stability, represented as $1 - \bar{Q}$ in (9).

The results are presented in Fig. 8. The equatorially trapped SST presents higher-frequency oscillations for both eastward and westward modes, but they are still located in the range of the MJO speed. Compared to the constant SST, the model with equatorially trapped SST presents wavelength selection for the growing mode, the SST distribution with an equatorial maximum can enhance the growth of the long eastward modes, while suppress the growth of the short westward modes (Fig. 8a). Of course, the ultraviolet catastrophe problem still exists for very short westward modes, for which this frictional skeleton model is not valid.

Associated with the equatorially trapped SST, the mean moisture, as well as the gross moisture statics stability, has also an equatorially trapped structure. For long eastward modes, the PBL Ekman pumping has an equatorially trapped structure (Fig. 6b), where the mean state moisture is also enough near the equator with a SST magnitude of 31°C, then the moisture convergence is enhanced, as well as the instability. On the other hand, for short westward modes, the maximum PBL Ekman pumping is in the off-equatorial region (Fig. 7a), where the mean state moisture is lower because the SST is cooler than that over the equator, thus the moisture convergence is relative weak compared to the constant SST.

When wavenumber is less than 10, it is interesting that the PBL prefers destabilizing the long modes (Fig. 8a), as the PBL has a wavelength-dependent Ekman pumping. When taking the lower-tropospheric moisture as a reference, Fig. 9 reveals that the relative moisture pumped by the PBL is weak for short waves. Since, for short waves, the wave activity is balanced largely by the wave convergence (Fig. 9), the perturbation pressure, which forces the Ekman pumping of (7), is relatively weak. However, for long waves, the retaining difference between the wave activity and wave convergence still produces strong perturbation pressure, which excites Ekman pumping and provides a strong instability source for the MJO.

This result means that the realistic equatorially trapped SST does help to provide a strong instability for long waves and prefers the eastward propagation of the MJO.

5. Discussion

The frictional skeleton model demonstrates the critical role of the planetary boundary layer (PBL) in

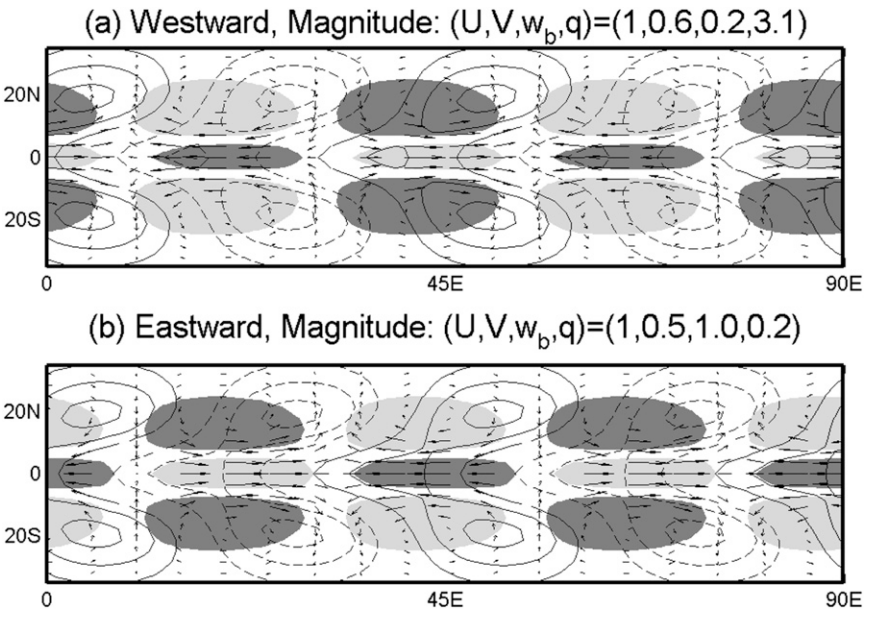

FIG. 7. As in Fig. 6, but for wavenumber 8.

sustaining the Madden–Julian oscillation (MJO) skeleton. The physical mechanism lies in the intrinsic characteristics of the equatorial waves and their associated PBL. On the planetary scale, the moisture convergence of the PBL is controlled mainly by the meridional variation of the pressure anomaly and is equatorially trapped and lies to the east of the MJO (Fig. 6b), thus the PBL Ekman pumping tends to moisten the low troposphere and precondition the atmosphere for deep convection of the MJO (Johnson et al. 1999). In future work we need to study these features in the observations. Hsu and Li (2012) also determined that the asymmetric moisture convergence in the PBL is helpful for the eastward propagation of the MJO, while the leading moisture convergence is mainly coming from the zonal wind convergence, since in their work the convection center was chosen in the off-equatorial region.

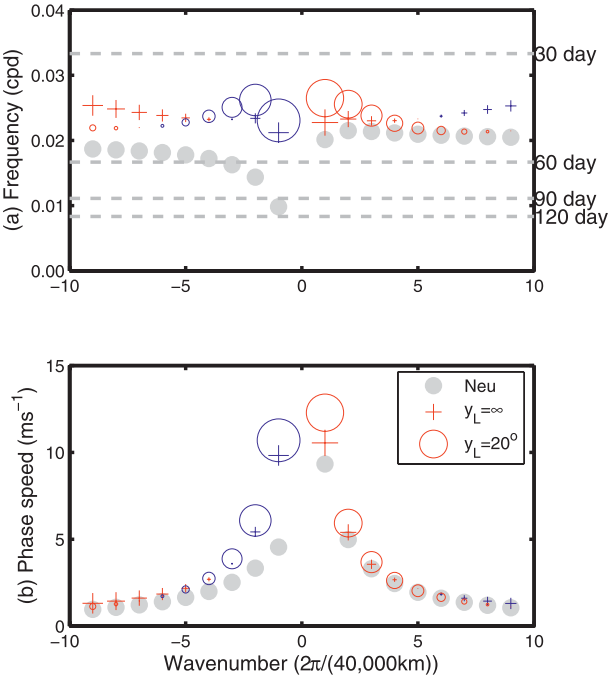

FIG. 8. As in Fig. 1, but red and blue denote constant and equatorially trapped SST, respectively. Gray dots represent the neutral mode of MS09. The maximum growth rate is 0.12 day^{-1}.

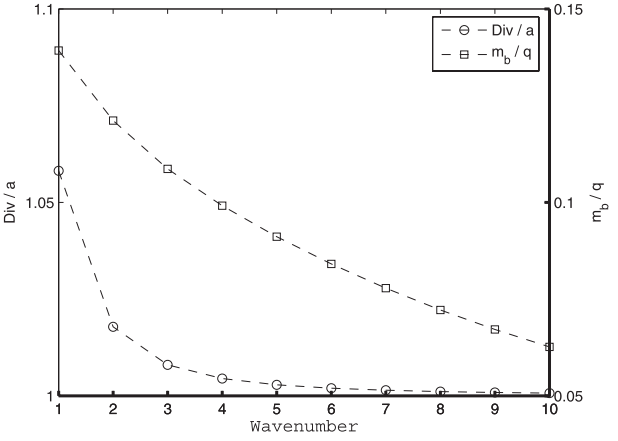

FIG. 9. Magnitude ratios of divergence to wave activity (Div/a) and Ekman pumping moisture to lower-tropospheric moisture (m_b/q) as a function of wavenumber.

The equatorially trapped sea surface temperature prefers coupling the long waves and provides a strong instability for eastward propagation of the MJO. During the boreal summer the mean state has strong off-equatorial moisture sources, such as in the South Asian monsoon region, where the off-equatorial moisture convergence in the PBL should be important (Wang and Xie 1997; Wang et al. 2005). The proposed frictional skeleton model may be instrumental to understanding the mechanism of the Indian monsoon intraseasonal oscillation.

Keep in mind that this frictional skeleton model is only valid for large-scale waves (MS09). Although it presents unrealistic unstable short westward modes, in the large-scale wave regime, this frictional skeleton model prefers the unstable planetary scales and selects the eastward propagation of the MJO.

Here we only include the role of scale interaction implicitly, which is parameterized as planetary-scale wave activity (MS09). Actually, the scale interaction between the MJO and synoptic-scale motions also provides instability sources for the MJO (Biello and Majda 2005; Wang and Liu 2011; Liu and Wang 2011, 2012; Liu et al. 2011). So it is necessary to find out how the PBL regulates the synoptic-scale motions, and their relations with the MJO. This calls for future theoretical, model, and observational studies.

Acknowledgments. This study was supported by the Climate Dynamics Program of the National Science Foundation under award AGS-1005599 and the Global Research Laboratory (GRL) Program from the Ministry of Education, Science, and Technology (MEST), South Korea. Additional support was provided by the Japan Agency for Marine-Earth Science and Technology (JAMSTEC), by NASA through Grant NNX07AG53G, and by NOAA through Grant NA17RJ1230 through their sponsorship of research activities at the International Pacific Research Center.

REFERENCES

Biello, J. A., and A. J. Majda, 2005: A new multiscale model for the Madden–Julian oscillation. *J. Atmos. Sci.,* **62,** 1694–1721.

——, ——, and M. W. Moncrieff, 2007: Meridional momentum flux and superrotation in the multi-scale IPESD MJO model. *J. Atmos. Sci.,* **64,** 1636–1651.

Frierson, D., A. J. Majda, and O. Pauluis, 2004: Large-scale dynamics of precipitation fronts in the tropical atmosphere: A novel relaxation limit. *Commun. Math. Sci.,* **2,** 591–626.

Gill, A. E., 1980: Some simple solutions for heat-induced tropical circulation. *Quart. J. Roy. Meteor. Soc.,* **106,** 447–462.

Haertel, P. T., and G. N. Kiladis, 2004: Dynamics of 2-day equatorial waves. *J. Atmos. Sci.,* **61,** 2707–2721.

Hendon, H. H., and B. Liebmann, 1994: Organization of convection within the Madden–Julian oscillation. *J. Geophys. Res.,* **99,** 8073–8084.

——, and M. L. Salby, 1994: The life cycle of the Madden–Julian oscillation. *J. Atmos. Sci.,* **51,** 2225–2237.

Houze, R. A., Jr., S. S. Chen, D. E. Kingsmill, Y. Serra, and S. E. Yuter, 2000: Convection over the Pacific warm pool in relation to the atmospheric Kelvin–Rossby wave. *J. Atmos. Sci.,* **57,** 3058–3089.

Hsu, P.-C., and T. Li, 2012: Role of the boundary layer moisture asymmetry in causing the eastward propagation of the Madden–Julian oscillation. *J. Climate,* **25,** 4914–4931.

Johnson, R. H., T. M. Rickenbach, S. A. Rutledge, P. E. Ciesielski, and W. H. Schubert, 1999: Trimodal characteristics of tropical convection. *J. Climate,* **12,** 2397–2418.

Jones, C., and B. C. Weare, 1996: The role of low-level moisture convergence and ocean latent heat fluxes in the Madden and Julian oscillation: An observational analysis using ISCCP data and ECMWF analyses. *J. Climate,* **9,** 3086–3104.

Khouider, B., and A. J. Majda, 2006: A simple multicloud parameterization for convectively coupled tropical waves. Part I: Linear analysis. *J. Atmos. Sci.,* **63,** 1308–1323.

——, and ——, 2007: A simple multicloud parameterization for convectively coupled tropical waves. Part II: Nonlinear simulations. *J. Atmos. Sci.,* **64,** 381–400.

——, and ——, 2008: Equatorial convectively coupled waves in a simple multicloud model. *J. Atmos. Sci.,* **65,** 3376–3397.

——, A. St-Cyr, A. J. Majda, and J. Tribbia, 2011: The MJO and convectively coupled waves in a coarse-resolution GCM with a simple multicloud parameterization. *J. Atmos. Sci.,* **68,** 240–264.

Kikuchi, K., and B. Wang, 2010: Spatiotemporal wavelet transform and the multiscale behavior of the Madden–Julian oscillation. *J. Climate,* **23,** 3814–3834.

Kiladis, G. N., K. H. Straub, and P. T. Haertel, 2005: Zonal and vertical structure of the Madden–Julian oscillation. *J. Atmos. Sci.,* **62,** 2790–2809.

——, M. C. Wheeler, P. T. Haertel, K. H. Straub, and P. E. Roundy, 2009: Convectively coupled equatorial waves. *Rev. Geophys.,* **47,** RG2003, doi:10.1029/2008RG000266.

Knutson, T. R., and K. M. Weickmann, 1987: 30–60-day atmospheric oscillation: Composite life cycles of convection and circulation anomalies. *Mon. Wea. Rev.,* **115,** 1407–1436.

Li, T., and B. Wang, 1994: The influence of sea surface temperature on the tropical intraseasonal oscillation: A numerical study. *Mon. Wea. Rev.,* **122,** 2349–2362.

——, and C. Zhou, 2009: Planetary-scale selection of the Madden–Julian oscillation. *J. Atmos. Sci.,* **66,** 2429–2443.

Lin, J., B. E. Mapes, M. Zhang, and M. Newman, 2004: Stratiform precipitation, vertical heating profiles, and the Madden–Julian oscillation. *J. Atmos. Sci.,* **61,** 296–309.

Liu, F., and B. Wang, 2011: A model for the interaction between the 2-day waves and moist Kelvin waves. *J. Atmos. Sci.,* **69,** 611–625.

——, and ——, 2012: Impacts of upscale heat and momentum transfer by moist Kelvin waves on the Madden–Julian oscillation: A theoretical model study. *Climate Dyn.,* doi:10.1007/s00382-011-1281-0, in press.

——, G. Huang, and L. Feng, 2011: Critical roles of convective momentum transfer in sustaining the multi-scale Madden–Julian oscillation. *Theor. Appl. Climatol.,* **108,** 471–477, doi:10.1007/s00704-011-0541-6.

Madden, R., and P. Julian, 1971: Detection of a 40-50 day oscillation in the zonal wind in the tropical Pacific. *J. Atmos. Sci.,* **28,** 702–708.

——, and ——, 1972: Description of global-scale circulation cells in the tropics with a 40-50 day period. *J. Atmos. Sci.,* **29,** 1109–1123.

——, and ——, 1994: Observations of the 40–50-day tropical oscillation—A review. *Mon. Wea. Rev.,* **122,** 814–837.

Majda, A. J., and J. A. Biello, 2004: A multiscale model for the intraseasonal oscillation. *Proc. Natl. Acad. Sci. USA,* **101,** 4736–4741.

——, and S. N. Stechmann, 2009a: A simple dynamical model with features of convective momentum transport. *J. Atmos. Sci.,* **66,** 373–392.

——, and ——, 2009b: The skeleton of tropical intraseasonal oscillations. *Proc. Natl. Acad. Sci. USA,* **106,** 8417–8422.

——, and ——, 2011: Nonlinear dynamics and regional variations in the MJO skeleton. *J. Atmos. Sci.,* **68,** 3053–3071.

——, ——, and B. Khouider, 2007: Madden–Julian oscillation analog and intraseasonal variability in a multicloud model above the equator. *Proc. Natl. Acad. Sci. USA,* **104,** 9919–9924.

Maloney, E. D., and D. L. Hartmann, 1998: Frictional moisture convergence in a composite life cycle of the Madden–Julian oscillation. *J. Climate,* **11,** 2387–2403.

Matsuno, T., 1966: Quasi-geostrophic motions in the equatorial area. *J. Meteor. Soc. Japan,* **44,** 25–43.

Matthews, A. J., 2000: Propagation mechanisms for the Madden–Julian oscillation. *Quart. J. Roy. Meteor. Soc.,* **126,** 2637–2651.

Moncrieff, M. W., 2004: Analytic representation of the large-scale organization of tropical convection. *J. Atmos. Sci.,* **61,** 1521–1538.

Moskowitz, B. M., and C. S. Bretherton, 2000: An analysis of frictional feedback on a moist equatorial Kelvin mode. *J. Atmos. Sci.,* **57,** 2188–2206.

Nakazawa, T., 1988: Tropical super clusters within intraseasonal variations over the western Pacific. *J. Meteor. Soc. Japan,* **66,** 823–839.

Ohuchi, K., and M. Yamasaki, 1997: Kelvin wave-CISK controlled by surface friction: A possible mechanism of super cloud cluster. Part I: Linear theory. *J. Meteor. Soc. Japan,* **75,** 497–511.

Roundy, P. E., and W. Frank, 2004: A climatology of waves in the equatorial region. *J. Atmos. Sci.,* **61,** 2105–2132.

Rui, H., and B. Wang, 1990: Development characteristics and dynamic structure of tropical intraseasonal convection anomalies. *J. Atmos. Sci.,* **47,** 357–379.

Salby, M. L., and H. H. Hendon, 1994: Intraseasonal behavior of clouds, temperature, and motion in the tropics. *J. Atmos. Sci.,* **51,** 2207–2224.

——, R. R. Garcia, and H. H. Hendon, 1994: Planetary-scale circulations in the presence of climatological and wave-induced heating. *J. Atmos. Sci.,* **51,** 2344–2367.

Slingo, A., P. Inness, R. Neale, S. Woolnough, and G.-Y. Yang, 2003: Scale interaction on diurnal to seasonal timescales and their relevance to model systematic errors. *Geophys. Ann.,* **46,** 139–155.

Sperber, K. R., 2003: Propagation and vertical structure of the Madden–Julian oscillation. *Mon. Wea. Rev.,* **131,** 3018–3037.

Straub, K. H., and G. N. Kiladis, 2003: Interactions between the boreal summer intraseasonal oscillation and higher-frequency tropical wave activity. *Mon. Wea. Rev.,* **131,** 945–960.

Tian, B., D. E. Waliser, E. J. Fetzer, B. H. Lambrigtsen, Y. L. Yung, and B. Wang, 2006: Vertical moist thermodynamic structure and spatial–temporal evolution of the MJO in AIRS observations. *J. Atmos. Sci.,* **63,** 2462–2485.

Waite, M. L., and B. Khouider, 2009: Boundary layer dynamics in a simple model for convectively coupled gravity waves. *J. Atmos. Sci.,* **66,** 2780–2795.

Wang, B., 1988: Dynamics of tropical low-frequency waves: An analysis of the moist Kelvin wave. *J. Atmos. Sci.,* **45,** 2051–2065.

——, and H. Rui, 1990: Dynamics of the coupled moist Kelvin–Rossby wave on an equatorial beta plane. *J. Atmos. Sci.,* **47,** 397–413.

——, and T. Li, 1994: Convective interaction with boundary layer dynamics in the development of the tropical intraseasonal system. *J. Atmos. Sci.,* **51,** 1386–1400.

——, and X. Xie, 1997: A model for the boreal summer intraseasonal oscillation. *J. Atmos. Sci.,* **54,** 72–86.

——, and F. Liu, 2011: A model for scale interaction in the Madden–Julian oscillation. *J. Atmos. Sci.,* **68,** 2524–2536.

——, P. J. Webster, and H. Teng, 2005: Antecedents and self-induction of active-break South Asian monsoon unraveled by satellites. *Geophys. Res. Lett.,* **32,** L04704, doi:10.1029/2004GL020996.

Wheeler, M., and G. N. Kiladis, 1999: Convectively coupled equatorial waves: Analysis of clouds and temperature in the wavenumber–frequency domain. *J. Atmos. Sci.,* **56,** 374–399.

Yang, B., X. Fu, and B. Wang, 2008: Atmosphere–ocean conditions jointly guide convection of the boreal-summer intraseasonal oscillation: Satellite observations. *J. Geophys. Res.,* **113,** D11105, doi:10.1029/2007JD009276.

Yano, J. I., and K. A. Emanuel, 1991: An improved model of the equatorial troposphere and its coupling to the stratosphere. *J. Atmos. Sci.,* **48,** 377–389.

Zhang, C., 2005: Madden–Julian oscillation. *Rev. Geophys.,* **43,** RG2003, doi:10.1029/2004RG000158.